AMD-Vol. 228

COMPUTATIONAL METHODS FOR SOLUTION OF INVERSE PROBLEMS IN MECHANICS

Presented at

THE 1998 ASME INTERNATIONAL MECHANICAL ENGINEERING
CONGRESS AND EXPOSITION
NOVEMBER 15–20, 1998
ANAHEIM, CALIFORNIA

Sponsored by

THE APPLIED MECHANICS DIVISION, ASME

Edited by

LORRAINE G. OLSON
UNIVERSITY OF NEBRASKA, LINCOLN

SUNIL SAIGAL
CARNEGIE MELLON UNIVERSITY
AND
NATIONAL SCIENCE FOUNDATION

THE AMERICAN SOCIETY OF MECHANICAL ENGINEERS
Three Park Avenue / New York, N.Y. 10016

AMD-Vol. 228, Computational Methods for Solution of
Inverse Problems in Mechanics
ASME 1998

SIMULTANEOUS DETERMINATION OF TEMPERATURES, HEAT FLUXES, DEFORMATIONS, AND TRACTIONS ON INACCESSIBLE BOUNDARIES

Brian H. Dennis and George S. Dulikravich
The Pennsylvania State University,
Department of Aerospace Engineering,
University Park, Pennsylvania 16802, U.S.A.
phone:(814)863-0134 fax:(814)865-7092 email:bhd102@psu.edu

ABSTRACT

A finite element method (FEM) formulation for the detection of unknown steady boundary conditions in heat conduction and linear elasticity and thermoelasticity continuum problems is presented. The present FEM formulation is capable of determining displacements, surface stresses, temperatures, and heat fluxes on the boundaries where such quantities are unknown or inaccessible, provided such quantities are sufficiently over-specified on other boundaries. Details of the discretization, linear system solution techniques, and sample results for 2-D problems are presented.

NOMENCLATURE

α	Coefficient of thermal expansion
$\{\delta\}$	Displacement vector
ϵ	strain
Γ	Boundary surface
λ	Lame's constant
Λ	Damping parameter
ν	Poisson's ratio
σ	Normal stress
$\bar{\sigma}$	Standard deviation
τ	Shear stress
Θ	Temperature
$\Delta\Theta$	difference between local and reference temperature
$[D]$	Damping matrix
E	Elastic modulus of elasticity
G	Shear modulus
k	Fourier coefficient of heat conduction
Q	Heat source
q	Heat flux
R	Uniform random number between 0 and 1
u, v, w	Deformations in the x, y, z directions
X, Y, Z	Body force in x, y, z directions
x, y, z	Cartesian body axes

FEM FORMULATION FOR THERMOELASTICITY

The Navier equations for linear static deformations u, v, w in three-dimensional Cartesian x, y, z coordinates are

$$(\lambda+G)\ (\tfrac{\partial^2 u}{\partial x^2}+\tfrac{\partial^2 v}{\partial x\partial y}+\tfrac{\partial^2 w}{\partial x\partial z})+G\nabla^2 u+X=0 \quad (1)$$

$$(\lambda+G)\ (\tfrac{\partial^2 u}{\partial x\partial y}+\tfrac{\partial^2 v}{\partial y^2}+\tfrac{\partial^2 w}{\partial y\partial z})+G\nabla^2 v+Y=0 \quad (2)$$

$$(\lambda+G)\ (\tfrac{\partial^2 u}{\partial x\partial z}+\tfrac{\partial^2 v}{\partial y\partial z}+\tfrac{\partial^2 w}{\partial z^2})+G\nabla^2 w+Z=0 \quad (3)$$

where,

$$\lambda=\frac{E\nu}{(1+\nu)(1-2\nu)},\quad G=\frac{E}{2(1+\nu)}$$

Here, X, Y, Z are body forces per unit volume due to stresses from thermal expansion.

$$X = -(3\lambda+2G)\frac{\partial\alpha\Delta\Theta}{\partial x} \quad (4)$$

$$Y = -(3\lambda+2G)\frac{\partial\alpha\Delta\Theta}{\partial y} \quad (5)$$

$$Z = -(3\lambda+2G)\frac{\partial\alpha\Delta\Theta}{\partial z} \quad (6)$$

This system of differential equations (1)-(3) can be written in the following matrix form

$$[L]^T([C][L]\{\delta\}-[C]\{\epsilon_0\})-\{f_b\}=0 \quad (7)$$

where the differential operator matrix, $[L]$, is defined as

$$[L]=\begin{bmatrix} \frac{\partial}{\partial x} & 0 & 0 \\ 0 & \frac{\partial}{\partial y} & 0 \\ 0 & 0 & \frac{\partial}{\partial z} \\ \frac{\partial}{\partial y} & \frac{\partial}{\partial x} & 0 \\ \frac{\partial}{\partial z} & 0 & \frac{\partial}{\partial x} \\ 0 & \frac{\partial}{\partial z} & \frac{\partial}{\partial y} \end{bmatrix} \quad (8)$$

and the elastic modulus matrix, $[C]$, is defined as

$$[C]=\frac{\lambda}{\nu}\begin{bmatrix} 1-\nu & \nu & \nu & 0 & 0 & 0 \\ \nu & 1-\nu & \nu & 0 & 0 & 0 \\ \nu & \nu & 1-\nu & 0 & 0 & 0 \\ 0 & 0 & 0 & \frac{1-2\nu}{2} & 0 & 0 \\ 0 & 0 & 0 & 0 & \frac{1-2\nu}{2} & 0 \\ 0 & 0 & 0 & 0 & 0 & \frac{1-2\nu}{2} \end{bmatrix} \quad (9)$$

Casting the system of equations (7) in integral form using the weighted residual method yields

$$\int_\Omega [V][L]^T([C][L]\{\delta\} - [C]\{\varepsilon_0\})\,d\Omega - \int_\Omega [V]\{f_b\}\,d\Omega = 0 \quad (10)$$

where the matrix, $[V]$, is the weight matrix which is a collection of test functions.

$$[V] = \begin{bmatrix} v_1 & 0 & 0 \\ 0 & v_2 & 0 \\ 0 & 0 & v_3 \end{bmatrix} \quad (11)$$

One should now integrate (10) by parts to get the weak form of (7)

$$\int_\Omega ([L][V]^T)^T[C][L]\{\delta\}\,d\Omega - \int_\Omega ([L][V]^T)^T[C]\{\varepsilon_0\}\,d\Omega - \int_\Omega [V]\{f_b\}\,d\Omega - \int_{\Gamma_1} [V]\{T\}\,d\Gamma = 0 \quad (12)$$

where $\{T\}$ is the vector of surface tractions on surface Γ_1.

$$\{T\} = [n][C][L]\{\delta\} \quad (13)$$

The matrix $[n]$ contains the Cartesian components of the unit vector normal to the surface Γ_1. The displacement field in the x, y, and z directions can now be represented with approximation functions

$$\delta_x(x,y,z) \approx \tilde{\delta}_x^e(x,y,z) = \sum_{i=1}^{n} N_i(x,y,z)u_i \quad (14)$$

$$\delta_y(x,y,z) \approx \tilde{\delta}_y^e(x,y,z) = \sum_{i=1}^{n} N_i(x,y,z)v_i \quad (15)$$

$$\delta_z(x,y,z) \approx \tilde{\delta}_z^e(x,y,z) = \sum_{i=1}^{n} N_i(x,y,z)w_i \quad (16)$$

Equations (14)-(16) can be rewritten in matrix form

$$\{\tilde{\delta}^e\} = [N]\{\delta^e\} \quad (17)$$

where $[N]$ is the interpolation matrix which contains the trial functions for each equation in the system. Also note that with Galerkin's method the weight matrix and the interpolation matrix are equal, $[N] = [V]^T$. If the matrix $[B]$ is defined as

$$[B] = [L][N] \quad (18)$$

then the substitution of the approximation functions (17) into the weak statement (12) creates the weak integral form for a finite element expressed as

$$\int_{\Omega^e} [B]^T[C][B]\{\delta^e\}\,d\Omega^e - \int_{\Omega^e} [B]^T[C]\{\varepsilon_0^e\}\,d\Omega^e - \int_{\Omega^e} [N]^T\{f_b^e\}\,d\Omega^e - \int_{\Gamma_1^e} [N]^T\{T^e\}\,d\Gamma^e = 0 \quad (19)$$

This can also be written in the matrix form as

$$[K^e]\{\delta^e\} = \{f^e\} \quad (20)$$

For thermal stresses, the initial elemental strain vector, ε_0^e, becomes

$$\{\varepsilon_0^e\} = \begin{bmatrix} \alpha\Delta\Theta & \alpha\Delta\Theta & \alpha\Delta\Theta & 0 & 0 & 0 \end{bmatrix}^T \quad (21)$$

The local stiffness matrix, $[K^e]$, and the force per unit volume vector, $\{f^e\}$, are determined for each element in the domain and then assembled into the global system

$$[K]\{\delta\} = \{F\} \quad (22)$$

After applying boundary conditions, the global displacements are found by solving this system of linear algebraic equations. The stresses, $\{\sigma\}$, can then be found in terms of the displacements, $\{\delta\}$

$$\{\sigma\} = [C][L]\{\delta\} - [C]\{\varepsilon_0\} \quad (23)$$

FEM FORMULATION FOR THERMAL PROBLEM

The temperature distribution throughout the domain can be found by solving Poisson's equation for steady linear heat conduction with a distributed steady heat source function, Q, and thermal conductivity coefficient, k.

$$-k\left(\frac{\partial^2\Theta}{\partial x^2} + \frac{\partial^2\Theta}{\partial y^2} + \frac{\partial^2\Theta}{\partial z^2}\right) = Q \quad (24)$$

Applying the method of weighted residuals to (24) over an element results in

$$\int_{\Omega^e} \left(\frac{\partial^2\Theta}{\partial x^2} + \frac{\partial^2\Theta}{\partial y^2} + \frac{\partial^2\Theta}{\partial z^2} - \frac{Q}{k}\right)v\,d\Omega^e = 0 \quad (25)$$

Integrating this by parts once (25) creates the weak statement for an element

$$-\int_{\Omega^e} k\left(\frac{\partial v}{\partial x}\frac{\partial\Theta}{\partial x} + \frac{\partial v}{\partial y}\frac{\partial\Theta}{\partial y} + \frac{\partial v}{\partial z}\frac{\partial\Theta}{\partial z}\right)d\Omega^e = \int_{\Omega^e} N_i Q\,d\Omega^e - \int_{\Gamma^e} N_i(q\cdot\hat{n})\,d\Omega^e \quad (26)$$

Variation of the temperature across an element can be expressed by

$$\Theta(x,y,z) \approx \tilde{\Theta}^e(x,y,z) = \sum_{i=1}^{m} N_i(x,y,z)\Theta_i \quad (27)$$

Using Galerkin's method, the weight function v and the interpolation function for Θ are chosen to be the same.
By defining the matrix $[B]$ as

$$[B] = \begin{bmatrix} \frac{\partial N_1}{\partial x} & \frac{\partial N_2}{\partial x} & \cdots & \frac{\partial N_m}{\partial x} \\ \frac{\partial N_1}{\partial y} & \frac{\partial N_2}{\partial y} & \cdots & \frac{\partial N_m}{\partial y} \\ \frac{\partial N_1}{\partial z} & \frac{\partial N_2}{\partial z} & \cdots & \frac{\partial N_m}{\partial z} \end{bmatrix} \quad (28)$$

the weak statement (26) can be written in the matrix form as

$$[K_c^e]\{\Theta^e\} = \{Q^e\} \quad (29)$$

where

$$[K_c^e] = \int_{\Omega^e} k[B]^T[B]\,d\Omega^e \tag{30}$$

$$\{Q^e\} = -\int_{\Omega^e} Q\{N\}\,d\Omega + \int_{\Gamma^e} q_s\{N\}\,d\Gamma^e \tag{31}$$

The local stiffness matrix, $[K_c^e]$, and heat flux vector, $\{Q^e\}$, are determined for each element in the domain and then assembled into the global system

$$[K_c]\{\Theta\} = \{Q\} \tag{32}$$

DIRECT AND INVERSE FORMULATIONS

The above equations for steady heat conduction and linear elasticity were discretized separately by using a Galerkin's finite element method. This results in two linear systems of algebraic equations

$$[K]\{\delta\} = \{F\}, \quad [K_c]\{\Theta\} = \{Q\} \tag{33}$$

These systems are large, sparse, symmetric, and positive definite. Once these global systems have been formed, the boundary conditions can be applied. For a well-posed (analysis or direct) problem, the boundary conditions must be known on all boundaries of the domain. For heat conduction, either the temperature, Θ, or the heat flux, Q, must be specified at each point of the boundary. For elasticity, the displacement vector components, U_s, V_s, W_s, or the surface traction vector components, $T_{x_s}, T_{y_s}, T_{z_s}$, must be specified on the entire boundary.

For inverse problems, the unknown boundary conditions on parts of the boundary can be determined by over-specifying the boundary conditions (enforcing both Dirichlet and Neumann type boundary conditions) on at least some of the remaining portions of the boundary, and providing either Dirichlet or Neumann type boundary conditions on the rest of the boundary. It is possible, after a series of algebraic manipulations, to transform the original system of equations into a system which enforces the over-specified boundary conditions and includes the unknown boundary conditions as a part of the unknown solution vector. This formulation is an adaptation of a method by Martin and Dulikravich (1996) for the inverse detection of boundary conditions in steady heat conduction and by Martin et al. (1995) for finding unknown boundary tractions and deformations in elastostatics using the boundary element method (BEM).

As an example, consider the linear system (32) for steady heat conduction on a quadrilateral finite element with boundary conditions given at points 1 and 4.

$$\begin{bmatrix} K_{11} & K_{12} & K_{13} & K_{14} \\ K_{21} & K_{22} & K_{23} & K_{24} \\ K_{31} & K_{32} & K_{33} & K_{34} \\ K_{41} & K_{42} & K_{43} & K_{44} \end{bmatrix} \begin{Bmatrix} \Theta_1 \\ \Theta_2 \\ \Theta_3 \\ \Theta_4 \end{Bmatrix} = \begin{Bmatrix} Q_1 \\ Q_2 \\ Q_3 \\ Q_4 \end{Bmatrix} \tag{34}$$

As an example of an inverse problem, one could specify both the temperature and the heat flux at point 1, flux only at points 2 and 3, and assume the boundary conditions at point 4 as being unknown. The original system of equations (34) can be modified by grouping all available boundary conditions in a vector on the right hand side

$$\begin{bmatrix} K_{12} & K_{13} & K_{14} & 0 \\ K_{22} & K_{23} & K_{24} & 0 \\ K_{32} & K_{33} & K_{34} & 0 \\ K_{42} & K_{43} & K_{44} & -1 \end{bmatrix} \begin{Bmatrix} \Theta_2 \\ \Theta_3 \\ \Theta_4 \\ Q_4 \end{Bmatrix} = \begin{Bmatrix} Q_1 - \Theta_1 K_{11} \\ Q_2 - \Theta_1 K_{21} \\ Q_3 - \Theta_1 K_{31} \\ 0 - \Theta_1 K_{41} \end{Bmatrix} \tag{35}$$

The same procedure can be applied to the system matrices for both heat steady conduction and elasticity in 2-D or 3-D. The resulting systems of equations will remain sparse, but will become unsymmetric and possibly rectangular depending on the ratio of the number of known to unknown boundary conditions. The next section will discuss techniques for solving such systems.

REGULARIZATION

Three regularization methods were applied separately to the solution of the systems of equations in attempts to increase the method's tolerance for measurement errors in the over-specifiedspecified boundary conditions. Here we consider the regularization of the inverse heat conduction problem.

The general form of a regularized system is given as (Neumaier, 1998):

$$\begin{bmatrix} K_c \\ \Lambda D \end{bmatrix} \{\Theta\} = \begin{Bmatrix} Q \\ 0 \end{Bmatrix} \tag{36}$$

The traditional Tikhonov regularization is obtained when the damping matrix, $[D]$, is set equal to the identity matrix. Solving (36) in a least squares sense minimizes the following error function.

$$error(\Theta) = ||[K_c]\{\Theta\} - \{Q\}||_2^2 + ||\Lambda[D]\{\Theta\}||_2^2 \tag{37}$$

This is the minimization of the residual plus a penalty term. The form of the damping matrix determines what penalty is used and the damping parameter, Λ, weights the penalty for each equation. These weights should be determined according to the error associated with the respective equation.

Method 1

This method of regularization uses a constant damping parameter Λ over the entire domain and the identity matrix as the damping matrix. This method can be considered the traditional Tikhonov method. The penalty term being minimized in this case is the square of the L_2 norm of the solution vector $\{x\}$. Minimizing this norm will tend to drive the components of $\{x\}$ to uniform values thus producing a smoothing effect. However, minimizing this penalty term will ultimately drive each component to zero, completely destroying the real solution. Thus, great care must be exercised in choosing the damping parameter Λ so that a good balance of smoothness and accuracy is achieved.

Method 2

This method of regularization uses a constant damping parameter Λ only for equations corresponding to the unknown boundary values. For all other equations $\Lambda = 0$ and $[D] = [I]$ since the largest errors occur at the boundaries where the temperatures and fluxes are unknown.

Method 3

This method uses Laplacian smoothing of the temperatures on the boundaries where the boundary conditions are unknown.

A penalty term could be constructed such that curvature of the solution is minimized along with the residual.

$$||\nabla^2 \Theta_{ub}||_2^2 \rightarrow \min \tag{38}$$

Eqn. (38) can be discretized using the method of weighted residuals to determine the damping matrix, $[D]$.

$$||[D]\Theta_{ub}||_2^2 = \int_\Gamma (\nabla^2 \Theta_{ub})^2 d\Gamma = ||[K_c]\Theta_{ub}||_2^2 \tag{39}$$

In two-dimensional planar problems, $[K_c]$ and $[D]$ can be thought of as an assembly of the linear or quadratic rod elements that make up the boundary of the object where the boundary conditions are unknown. The main advantage of this method its ability to smooth the solution vector without necessarily driving the components to zero and away from the true solution.

SOLUTION OF THE LINEAR SYSTEM

In general, the resulting FEM systems for the inverse thermoelastic problems are sparse, unsymmetric, and often rectangular. These properties make the process of finding a solution to the system very challenging. Three approaches will be discussed here.

The first is to normalize the equations by multiplying both sides by the matrix transpose and solve the resulting square system with common sparse solvers.

$$[K]^T[K]\{\delta\} = [K]^T\{F\} \tag{40}$$

This approach has been found to be effective for certain inverse problems (Boschi and Fischer, 1996). The resulting normalized system is less sparse than the original system, but it is square, symmetric, and positive definite with application of regularization. The normalized system is solved with a direct method (Cholesky or LU factorization) or with an iterative method (preconditioned Krylov subspace). There are several disadvantages to this approach. Among them being the computation expense of computing $[K]^T[K]$, the large in-core memory requirements, and the roundoff error incurred during the $[K]^T[K]$ multiplication.

A second approach is to use iterative methods suitable for unsymmetrical and least squares problems. One such method is the LSQR method, which is an extension of the well-known conjugate gradient method (Paige and Saunders, 1982). The LSQR method and other similar methods such as the conjugate gradient for least squares (CGLS) solve the normalized system, but without explicit computation of $[K]^T[K]$. However, convergence rates of these methods depend strongly on the condition number of the normalized system which is roughly the condition number of $[K]$ squared. Convergence can be slow when solving the systems resulting from the inverse finite element discretization since they are ill-conditioned.

A third approach is to use a non-iterative method for unsymmetrical and least squares problems such as QR factorization or SVD (Golub and Van Loan, 1996). However, sparse implementations of QR or SVD solvers are needed to reduce the in-core memory requirements for the inverse finite element problems.

NUMERICAL RESULTS

The accuracy and efficiency of the finite element inverse formulation was tested on several simple two-dimensional problems with known analytic solutions. The method was implemented in an object-oriented finite element code written in C++. Elements used in the calculations were triangles with linear and quadratic interpolation functions. The triangular meshes were generated by an automatic Delauney triangulation technique (Shewchuk, 1996). Three different solution techniques were tested: a sparse QR factorization (Matstoms, 1991), a CGLS and LSQR code, and a CG solver applied to solving the normalized equations. The two basic test geometries included a rectangular plate and an annular disk (Fig. 1).

For heat conduction, one analytical test problem consisted of a rectangular homogeneous plate with uniform temperatures specified at the opposite boundaries and adiabatic conditions specified at the remaining two opposite boundaries. The FEM solution of this direct problem was less than 1% in error compared to the analytical solution. Another simple test case was steady heat conduction in an annular homogeneous disk. In a direct (well-posed) problem a uniform temperature of 50.0 K was enforced on the inner circular boundary while a temperature of 10.0 K was enforced on the outer circular boundary. The temperature field computed with the FEM had a maximum error of 1% compared to the analytical solution.

For elasticity, one analytical test problem consisted of a rectangular homogeneous plate under uniform tension at one end while having a fixed opposite boundary and zero tractions on the side walls. The FEM solution of this direct problem was less than 1% in error. Another elasticity test case was also utilized where an annular pressure vessel was used to test the FEM code (Martin et al., 1995). The FEM solution of a direct problem was obtained when specifying tractions on both the inner and the outer circular boundaries. The computed stress distributions were less than 2% in error compared to the analytical solution (Dennis and Dulikravich, 1998).

Next, combined thermoelastic analysis and inverse problem were attempted on an annular disk shown in Fig. 1. The outer circular boundary was constructed with 60 points while 30 points were used for the inner boundary. The triangular mesh contained 574 nodes and 242 quadratic elements. For the analysis problem, a temperature of 50.0 K was specified on the outer circular boundary and 10.0 K was specified on the inner circular boundary. Simultaneously, a tensile surface stress of 101.0 kPa was specified on the outer circular boundary and a tensile stress of 202.0 kPa was specified on the inner circular boundary. The following material properties were used: $E = 2 \times 10^3$ Pa, $\nu = 2 \times 10^{-1}$, $\alpha = 2 \times 10^{-3}$ K^{-1}, $k = 1\ Wm^{-1}K^{-1}$. The computed temperature and stress distributions are shown in Figs. 3,5,7.

The inverse problem was then created by over-specifying the outer circular boundary with the double-precision values of temperatures, fluxes, displacements, and tractions obtained from the analysis case. At the same time, no boundary conditions were specified on the inner circular boundary (Martin and Dulikravich, 1996). A damping parameter of $\Lambda = 0$ was used. The computed temperature and stress distributions are shown in Figs. 4,6,8. The maximum relative differences in temperatures, displacements, and stresses between the analysis and inverse results are less than 0.1% when solved with a QR factorization.

As a second thermoelastic test case, an analysis and inverse problem were solved on the domain shown in Fig. 2. The domain is composed of 16 internal holes, each with 15 nodes. The outer circular boundary was constructed with 250 points. The

triangular mesh contained 2310 nodes and 4170 linear elements.

For the analysis problem, a temperature of 1000.0 K was specified on the outer circular boundary and 50.0 K was specified on the inner circular boundaries. A pressure of 101.0 kPa was applied to the outer boundary while a pressure of 202.0 kPa was applied to each of the inner boundaries. The following material properties were used: $E = 2 \times 10^6$ Pa, $\nu = 10^{-1}$, $\alpha = 10^{-6}$ K^{-1}, $k = 1\ Wm^{-1}K^{-1}$. The computed temperature and stress distributions from this well- posed (direct or analysis) problem are shown in Figs. 9,11,13.

For the inverse problem, the boundary temperatures, fluxes, displacements, and tractions obtained from the forward analysis were specified on the outer circular boundary. No boundary conditions were specified on any of the inner circular boundaries. Regularization method 3 was used. A damping parameter of $\Lambda = 1 \times 10^{-8}$ was used when determining the temperature field and $\Lambda = 1 \times 10^{-4}$ was used when computing the displacement field. The computed temperature and stress distributions from this ill-posed (inverse) problem are shown in Figs. 10,12,14. The average relative differences between the forward and inverse temperatures, displacements, and stresses were less than 0.1% when solved using a QR factorization.

The inverse heat conduction problem on the annular disk and multiply-connected domain problems were tested with random measurement errors in the over-specified temperatures and fluxes. Random errors in the known boundary temperatures and fluxes were generated using the following equations (Martin and Dulikravich, 1996):

$$\Theta = \Theta_{bc} \pm \sqrt{-2\bar{\sigma}^2 \ln R} \quad (41)$$

$$q = q_{bc} \pm \sqrt{-2\bar{\sigma}^2 \ln R} \quad (42)$$

For each case, Eqns. (41)-(42) were used to generate errors in both the known boundary fluxes and temperatures obtained from the forward solution.

For the annular disk case, Figs. 15,16,17 show the effect of the standard deviation, $\bar{\sigma}$, and damping parameter, Λ, on the average error of the temperatures recovered on the unknown boundaries compared to the temperatures given by the forward solution. Regularization method 3 gave the best results for all values of $\bar{\sigma}$ producing error in the unknown boundary conditions of the same magnitude as the error in the known boundary conditions.

For the multiply-connected domain case, Figs. 18,19,20 show the effect of the standard deviation, $\bar{\sigma}$, and damping parameter, Λ, on the average error of the temperatures recovered on the unknown boundaries compared to the values given by the forward solution. None of the regularizations methods worked well with this case when measurement errors were applied. The errors in the known boundary conditions were amplified by several orders of magnitude in the recovered temperatures on the unknown boundary. These results indicate that this FEM inverse method requires better regularization if measurement errors are used with complicated geometries.

CONCLUSIONS

All three sparse matrix solvers performed well for test cases with relatively small number of variables. The QR factorization was found to provide the highest accuracy in the shortest amount of computing time. For each of the test problems presented here the total solution time was less than 5 seconds on a Pentium 200 MHz PC. However, the QR factorization failed for larger problems where the number of grid points was greater than about 2000. This is most likely due to the instability of the QR algorithm when dealing with systems with high condition numbers (Golub and Van Loan, 1996). Applying small amounts of regularization ($\Lambda > 10^{-16}$) to the sparse matrix eliminated the instability. The CG method applied to the normalized equations worked well for problems with less than 100 nodes. For more than 100 nodes, this method required many iterations to converge to a solution less accurate than the QR solution. When regularization was applied to the sparse matrix, the CG convergence improved dramatically but the QR factorization was much faster by comparison. The CGLS and LSQR methods were found to be slow for problems with more than 500 nodes, but was able to provide better solutions than those obtained with the CG applied to the normal equations.

ACKNOWLEDGMENTS

The authors are grateful for the National Science Foundation Grant DMI-9522854 monitored by Dr. George Hazelrigg, the NASA Lewis Research Center Grant NAG3-1995 facilitated by Dr. John Lytle and supervised by Dr. Kestutis Civinskas, and for ALCOA Foundation Faculty Research Award facilitated by Dr. Yimin Ruan and Dr. Owen Richmond.

REFERENCES

Boschi, L. and Fischer, R. P., 1996, "Iterative solutions for tomographic inverse problems: LSQR and SIRT," Tech. Rep. Seismology, Harvard University, Cambridge, MA.

Dennis, B. H. and Dulikravich, G. S., 1998, "A finite element formulation for the detection of boundary conditions in elasticity and heat transfer," In: *Proc. of Internat. Symposium on Inverse Problems in Eng. Mechanics*, ed. M. Tanaka, Nagano, Japan.

Golub, G. H. and Van Loan, C. F., 1996, *Matrix Computations*, 3rd edn., Johns Hopkins, Baltimore, MD.

Martin, T. J. and Dulikravich, G. S., 1996, "Inverse determination of boundary conditions in steady heat conduction," *ASME Journal of Heat Transfer*, Vol. 3, No. 118, pp. 546–554.

Martin, T. J., Halderman, J., and Dulikravich, G. S., 1995, "An inverse method for finding unknown surface tractions and deformations in elastostatics," *Computers and Structures*, Vol. 56, No. 5, pp. 825–836.

Matstoms, P., 1991, "The multifrontal solution of sparse least squares problems," Ph.D. Thesis, Linköping University, Sweden.

Neumaier, A., 1998, "Solving ill-conditioned and singular linear systems: A tutorial on regularization," to appear in *SIAM Review*.

Paige, C. C. and Saunders, M. A., 1982, "LSQR: An algorithm for sparse linear equations and sparse least squares," *ACM Transactions on Mathematical Software*, Vol. 8, No. 1, pp. 43–71.

Shewchuk, J. R., 1996, "Triangle: Engineering a 2D quality mesh generator and Delaunay triangulator," In: *First Workshop on Applied Computational Geometry*, Philadelphia, PA.

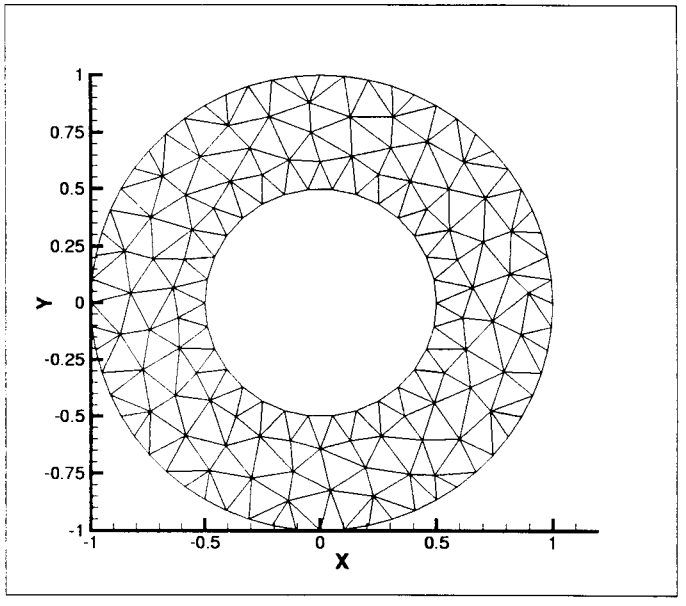

Figure 1: Triangular mesh for an annular disk test case geometry

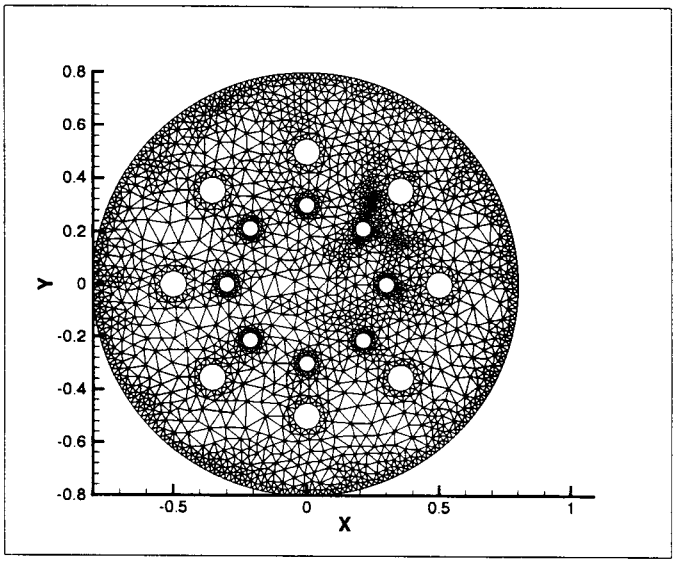

Figure 2: Triangular mesh for a multiply-connected domain test case geometry

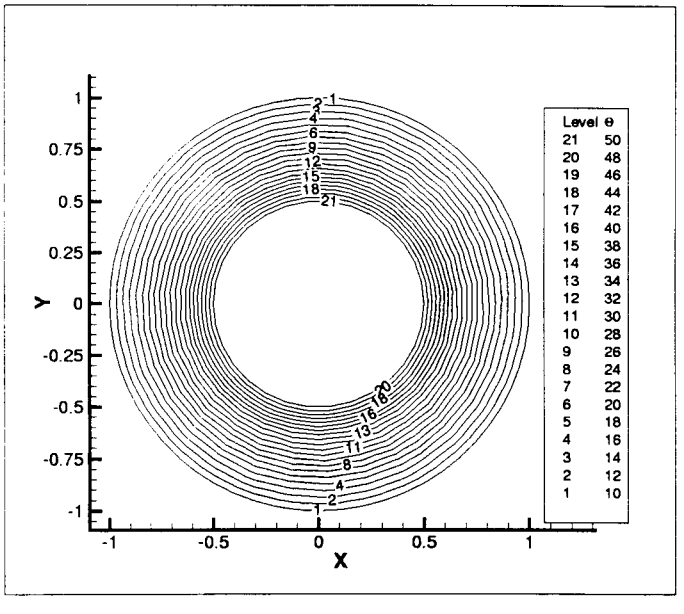

Figure 3: Computed isotherms with inner and outer boundary temperatures specified

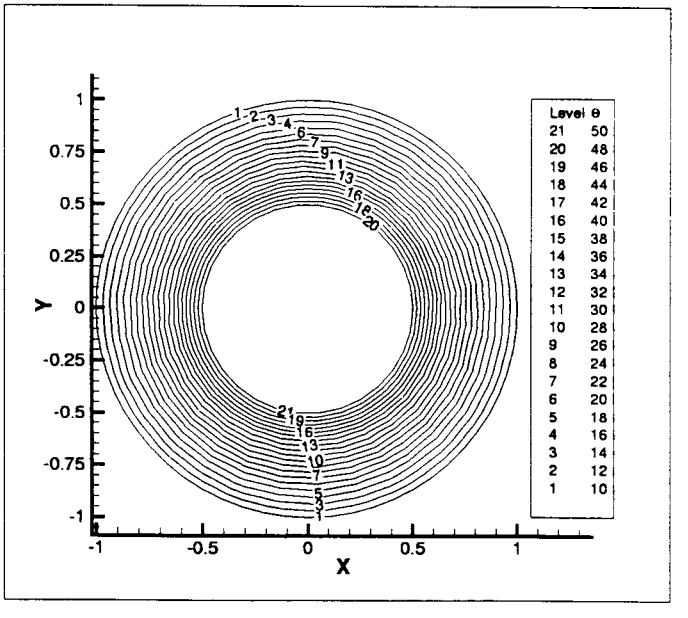

Figure 4: Computed isotherms with outer boundary temperatures and fluxes specified

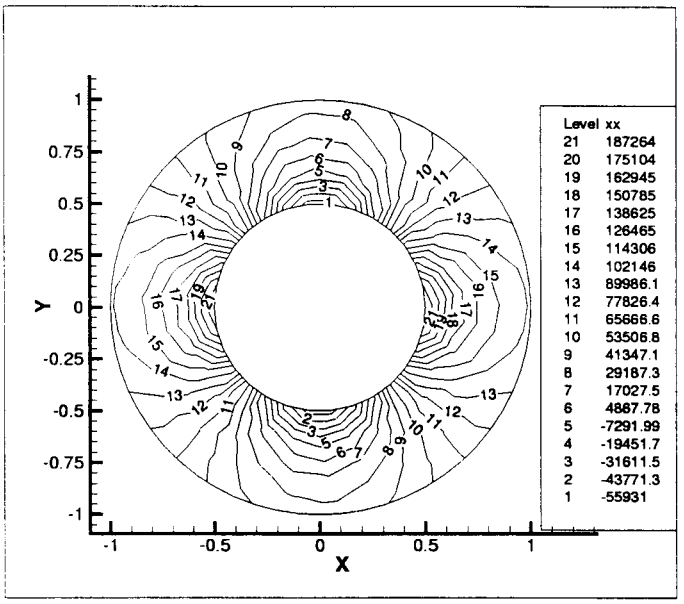

Figure 5: Computed normal stress distribution with inner and outer boundary tractions specified

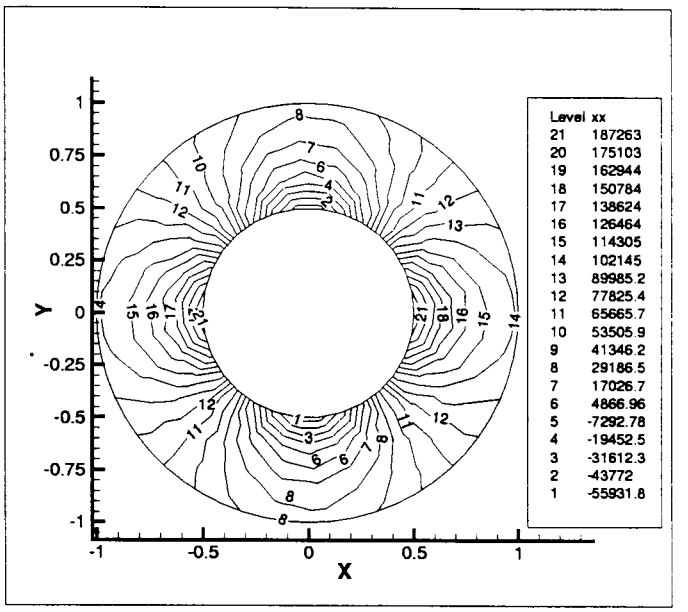

Figure 6: Computed normal stress distribution with outer boundary tractions and displacements specified

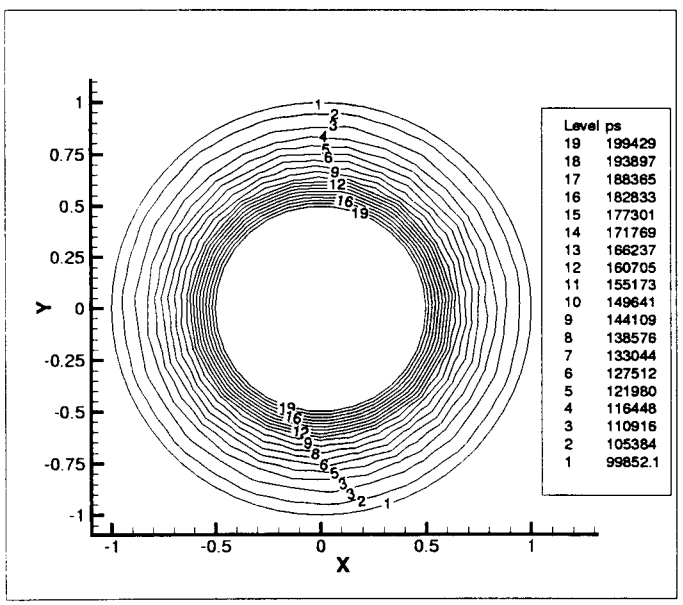

Figure 7: Computed principal stress distribution with inner and outer boundary tractions specified

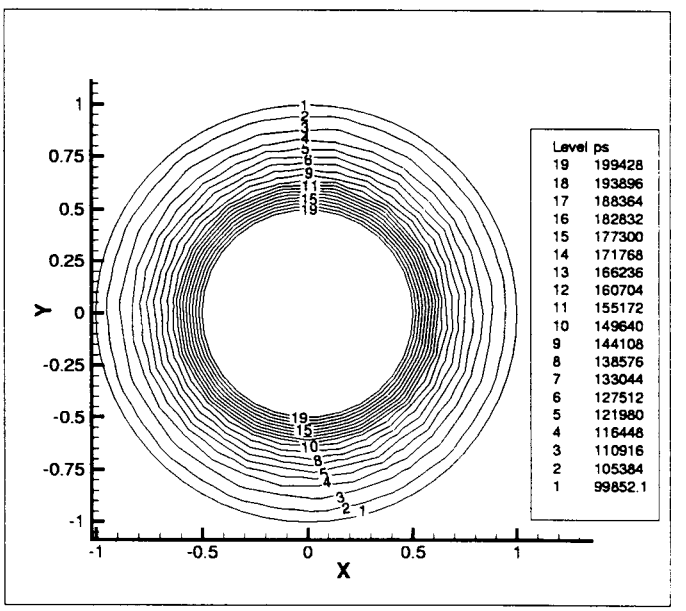

Figure 8: Computed principal stress distribution with outer boundary tractions and displacements specified

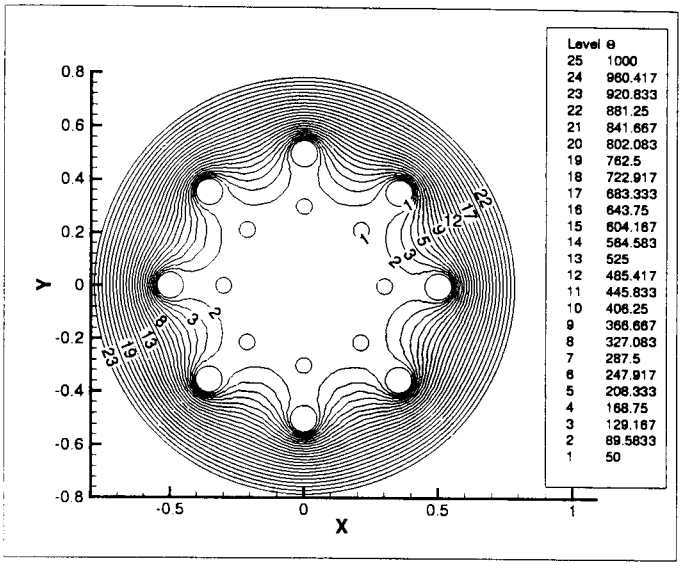

Figure 9: Computed isotherms with inner and outer boundary temperatures specified

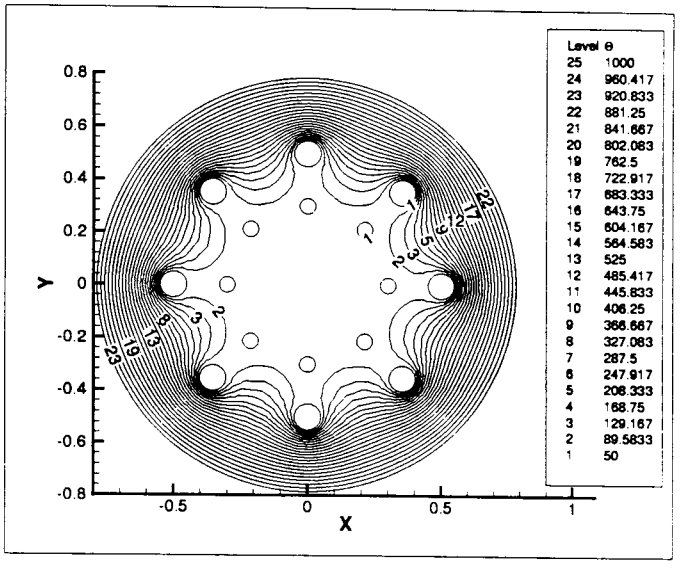

Figure 10: Computed isotherms with outer boundary temperatures and fluxes specified

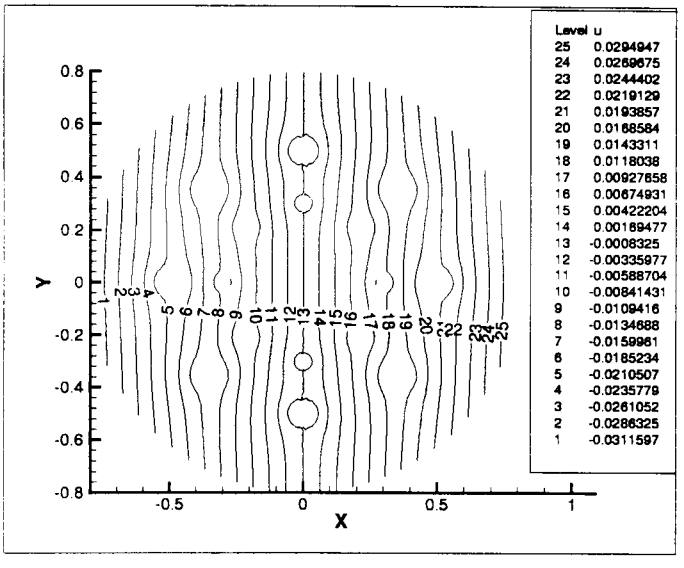

Figure 11: Computed displacements in x direction with inner and outer boundary tractions specified

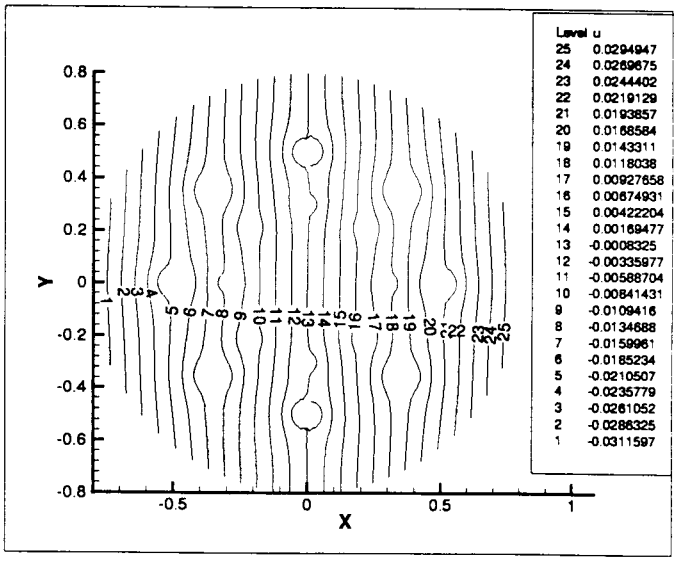

Figure 12: Computed displacements in x direction with outer boundary tractions and displacements specified

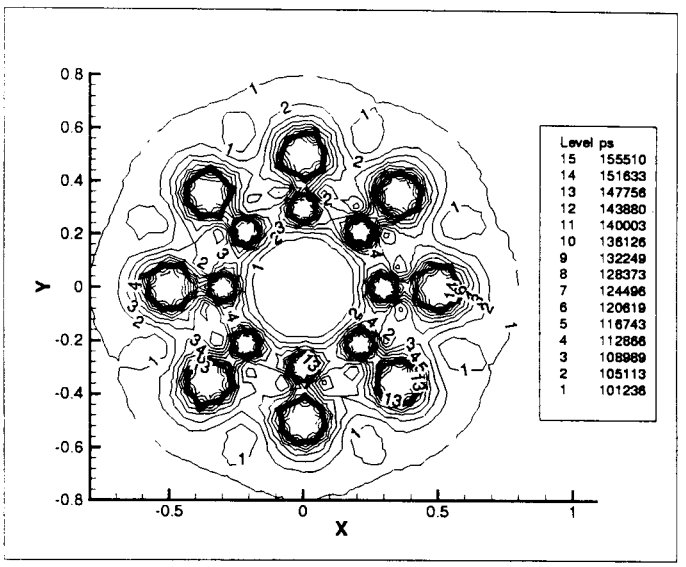

Figure 13: Computed principal stress distribution with inner and outer boundary tractions specified

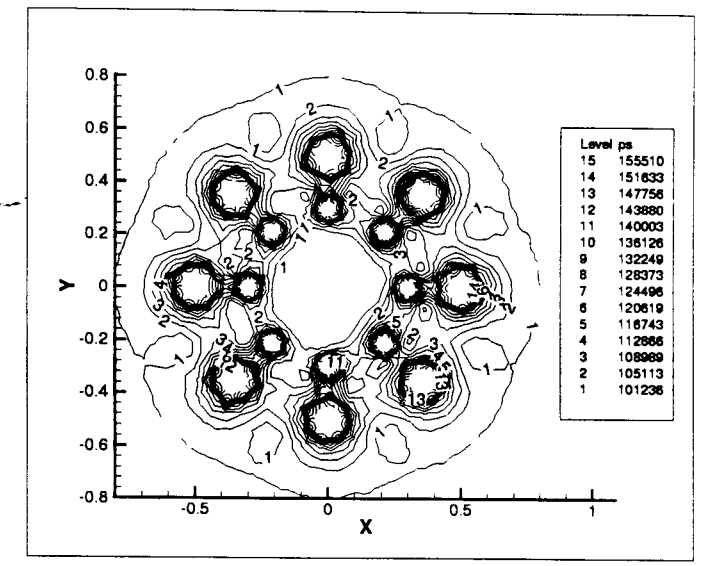

Figure 14: Computed principal stress distribution with outer boundary tractions and displacements specified

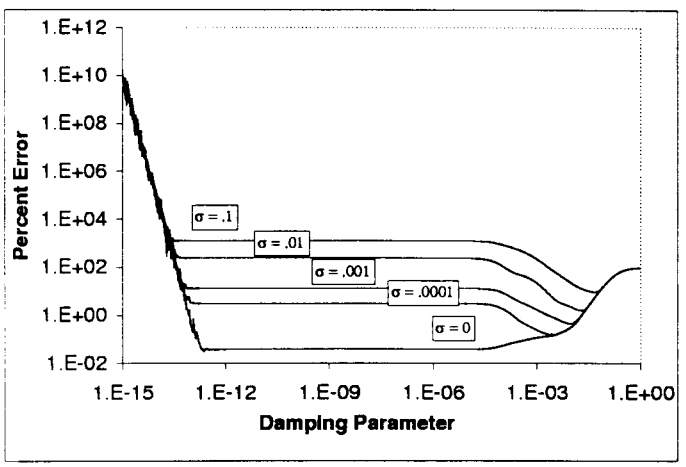

Figure 15: Average percent error of predicted temperatures on unknown boundaries for regularization method 1 on annular region

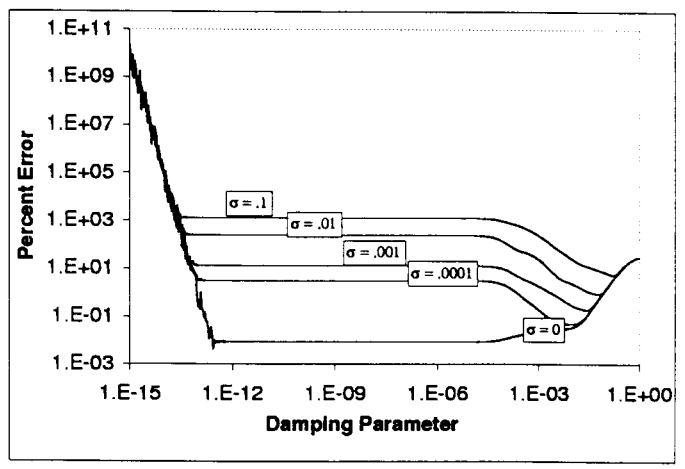

Figure 16: Average percent error of predicted temperatures on unknown boundaries for regularization method 2 on annular region

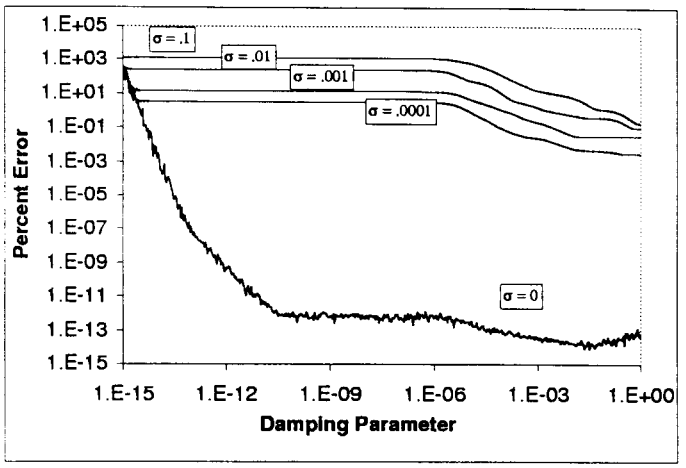

Figure 17: Average percent error of predicted temperatures on unknown boundaries for regularization method 3 on annular region

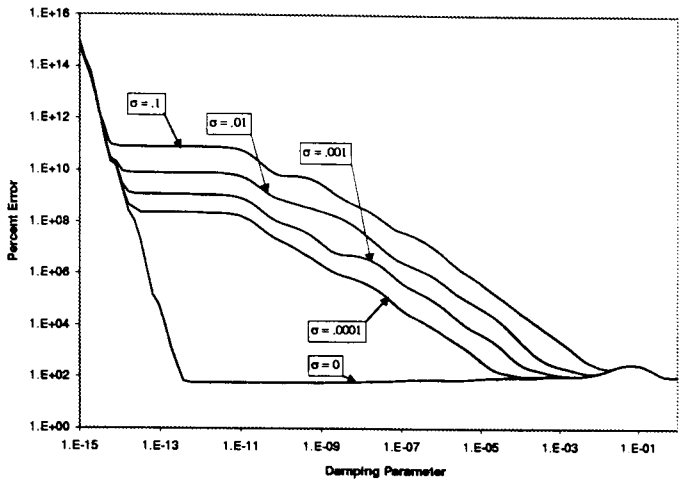

Figure 18: Average percent error of predicted temperatures on unknown boundaries for regularization method 1 on multiply-connected domain

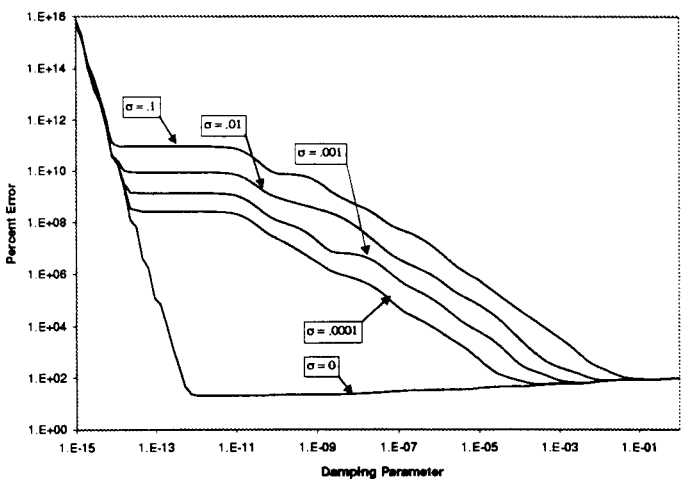

Figure 19: Average percent error of predicted temperatures on unknown boundaries for regularization method 2 on multiply-connected domain

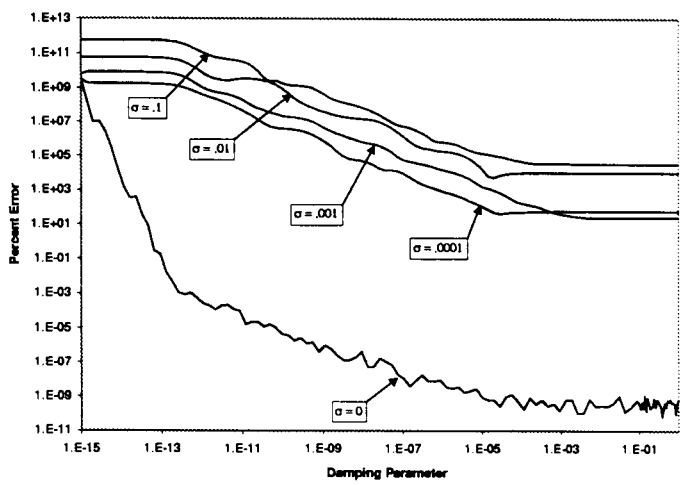

Figure 20: Average percent error of predicted temperatures on unknown boundaries for regularization method 3 on multiply-connected domain